Electronic Supplementary Material (ESI) for JAAS.

Supporting Information

Antiscattering X-ray fluorescence analysis for large-area samples

Wenyang Zhao[1,2], Keiichi Hirano[3], and Kenji Sakurai[2,1,a)]

[1]*University of Tsukuba, 1-1-1, Tennodai, Tsukuba, Ibaraki, 305-0006, Japan*

[2]*National Institute for Materials Science, 1-2-1, Sengen, Tsukuba, Ibaraki, 305-0047, Japan*

[3]*Institute of Materials Structure Science, High Energy Accelerator Research Organization, 1-1, Oho, Tsukuba, Ibaraki, 305-0801, Japan*

a) Corresponding Author, sakurai@yuhgiri.nims.go.jp

I. **X-ray fluorescence spectra of other certified reference materials**

Figure S1 shows the XRF spectra of a certified reference material (CRM), NIST 1515, apple leaves. To prepare the sample, the original material was mixed into cellulose powders at a mass fraction of 30%, and then the mixture was pressed into a pellet with a density of 1.5 g/cm^3. The spectra in Fig. S1(a) were measured in the synchrotron polarized experiment. The live time was 2 h. The spectra in Fig. S1(b) were measured in the laboratory unpolarized experiment. The live time was 10 min. On the basis of previous certified composition reports, the pellet sample was inferred to include 0.49% potassium, 0.46% calcium, approximately 8 ppm titanium, 15 ppm manganese, 25 ppm iron, and 0.3 ppm nickel. In Fig. S1(a), even though the spectra were unsuitable for quantitative analysis owing to the limited counting statistics, the above trace elements of low concentration could still be detected and identified. It was noted that the pellet sample also included 0.07 ppm vanadium and 0.03 ppm cobalt, of which the K lines were in the detectable X-ray energy range. However, these two elements were not detected owing to the minimum detectable limit. This experiment verified the feasibility of adopting the present experimental scheme in the detection of trace elements in low-Z matrices of environmental samples.

Figure S2 shows the X-ray fluorescence spectra of a CRM, JSAC 0615. This was a plastic disk that included toxic heavy metals. The certified composition of the metals was 212 ppm chromium, 43 ppm cadmium, and 202 ppm lead. In the spectra, lead was not observed because its K lines or L lines were not excited by the primary X-rays. Cadmium was not detected either because its L lines are inherently weak and easily absorbed in the plastic matrix. Chromium was easily detected. In Fig. S2(a), the Kα line was even stronger than the intensity of the scattering X-rays from the entire plastic matrix. In addition, two other trace elements, iron and cobalt, were detected. These two elements were probably contaminants during sample preparation or storage. This experiment verified the feasibility of adopting the present experimental scheme in the detection of trace toxic metals in plastic products, which is frequently a public health concern.

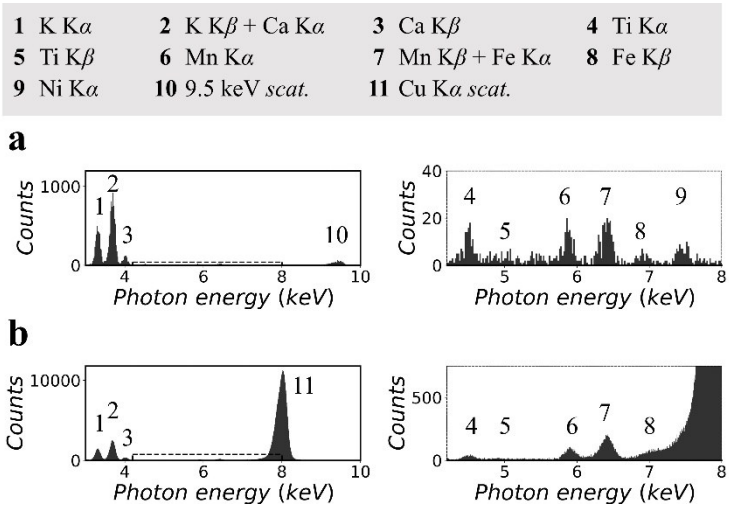

Figure S1. X-ray fluorescence spectra of CRM, NIST 1515, apple leaves. Original material was mixed into cellulose matrix at mass fraction of 30%. (a) measured in synchrotron polarized experiment, and (b) measured in laboratory unpolarized experiment. Details of spectra were enlarged and attached to right side.

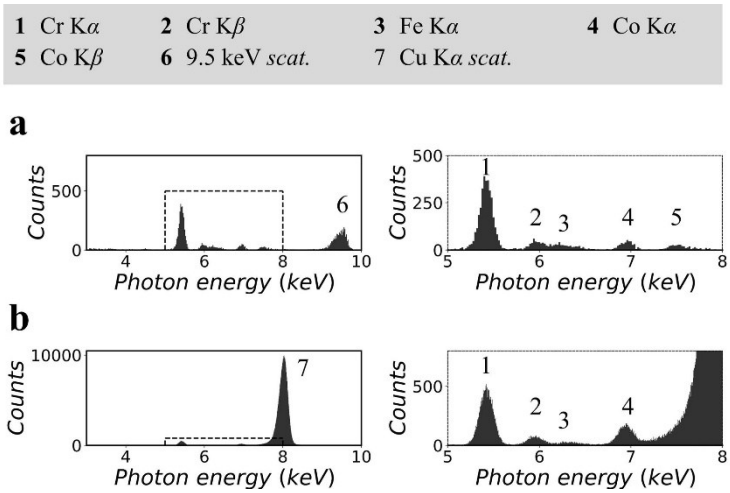

Figure S2. X-ray fluorescence of CRM JSAC 0615. (a) measured in synchrotron polarized experiment, and (b) measured in laboratory unpolarized experiment. Details of spectra are enlarged and attached on the right.

II. Calculation of scattering intensity

The calculation here only considers the differential cross section of coherent scattering and Compton scattering from an electron because this physical process determines the fact that the angular distribution of the scattering intensity has a sharp minimum in the direction of polarization. The calculation result is in the form of the cross section of scattering, including coherent scattering and Compton scattering, and is an average of the cross section of scattering from every point in the probing area on the sample. The average scattering cross section is denoted by $\bar{\sigma}_{scat}$. In addition, as the effective solid angle Ω of the capillaries determines the detectable fluorescence intensity, it is necessary to normalize $\bar{\sigma}_{scat}$ by Ω. The resulting $\bar{\sigma}_{scat}/\Omega$ is considered to be inversely proportional to the signal-to-background ratio in the XRF spectra. It is noted that the scattering intensity in an actual experiment is influenced by many other factors such as the scattering from an atom (atomic form factor for coherent scattering and incoherent scattering function for Compton scattering) and absorption in the sample matrix. However, when the radius-to-length of the capillaries is small enough, these factors have little influence on the final conclusion, and therefore they are not included in the calculation model for simplicity.

A *cartesian* coordinate system is introduced to describe the geometry in this problem. The primary X-rays propagate along the *z*-axis. For polarized X-rays, the polarization is along the *x*-axis. The observation direction of the scattering X-rays is described by two angles, θ and ϕ, where θ is the polar angle between the *z*-axis and the observation direction, and ϕ is the azimuth angle between the *x*-axis and the projection of the observation direction in the *x*-*y* plane. The differential cross sections of scattering from an electron are given by

$$\left(\frac{d\sigma}{d\Omega}\right)_{coh} = r_e^2\left(1 - \sin^2\theta\cos^2\phi\right)\#(S1a)$$

and

$$\left(\frac{d\sigma}{d\Omega}\right)_{Comp} = r_e^2\left(\frac{k}{k_0}\right)^2\frac{\left(\frac{k}{k_0} + \frac{k_0}{k} - 2\sin^2\theta\cos^2\phi\right)}{2}.\#(S1b)$$

where $(d\sigma/d\Omega)_{coh}$ denotes the differential cross section of coherent scattering, $(d\sigma/d\Omega)_{Comp}$ denotes the differential cross section of Compton scattering, r_e denotes the classical electron radius and equals 2.82×10^{-5} Å, and k_0 and k denote the wave vectors of the primary X-rays and scattering X-rays, respectively. The ratio of k and k_0 is given by

$$\frac{k}{k_0} = \frac{1}{1 + \frac{E_0}{m_e c^2}(1 - \cos\theta)}, \#(S2)$$

where E_0 denotes the photon energy of the primary X-rays, m_e denotes the electron mass, and c denotes the speed of light. It is noted that k/k_0 does not equal unity when $\theta = \pi/2$. Therefore, $(d\sigma/d\Omega)_{Comp}$ is not zero even when the observation direction is in the direction of polarization. On the other hand, as k/k_0 is dependent on E_0, this calculation relies on an assumed primary X-ray energy. Here, E_0 is set as 9.5 keV.

To clarify the role of the DOP, the primary X-ray beam is assumed to be a combination of two linearly polarized components: a parallel component and a perpendicular component. The polarization direction of the parallel component and the perpendicular component is parallel and perpendicular to the capillary axis of the collimator plate, respectively, as shown in Fig. S3 and Fig. S4. When the DOP of the primary X-ray beam is p, the percentage of the parallel component is $(1 + p)/2$, and the percentage of the perpendicular component is $(1 - p)/2$. The radius of the capillaries is r, and the length of the capillaries, *i.e.*, the thickness of the collimator plate, is t. For each capillary, the viewing area on the sample can be equivalently treated as a circular disk S_1 at one end of the capillary, and the corresponding active opening area on the detector can be equivalently treated as a circular disk S_2 at the other end. The radii of S_1 and S_2 are both r.

In the calculation, the cross section of scattering X-rays emitted from an area element dS_1 at P_1 on S_1 and detected by an area element dS_2 at P_2 on S_2 is first considered. The positions of P_1 and P_2 are described by polar coordinates for S_1 and S_2, which are (ρ_1,α_1) and (ρ_2,α_2), respectively. Here, ρ_i is defined as the length of $\vec{O_iP_i}$, and α_i is defined as the rotation angle from the *z*-axis to $\vec{O_iP_i}$, where $i = 1, 2$. The corresponding area element is

$$dS_1 = \rho_1 \, d\rho_1 \, d\alpha_1, \#(S3a)$$

and

$$dS_2 = \rho_2 \, d\rho_2 \, d\alpha_2. \#(S3b)$$

In the calculation of the parallel components, as shown in Fig. S3, for the scattering X-rays from P_1 to P_2, the observation direction in the *cartesian* coordinate system is described as

$$x = t, \#(S4a)$$
$$y = \rho_2 \sin\alpha_2 - \rho_1 \sin\alpha_1, \#(S4b)$$
$$z = \rho_2 \cos\alpha_2 - \rho_1 \cos\alpha_1. \#(S4c)$$

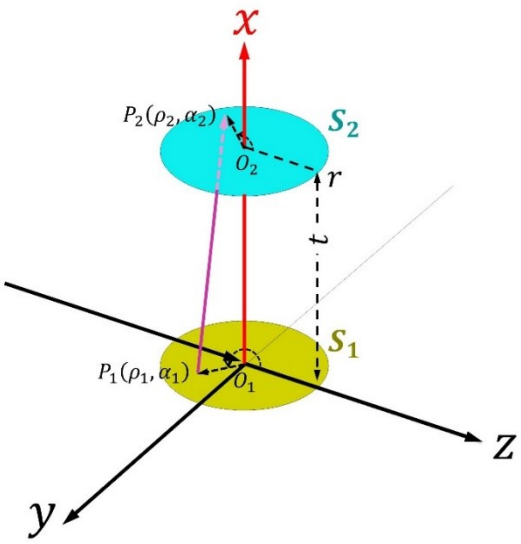

Figure S3. Calculation of parallel components in primary X-ray beam. Polarization is parallel to capillary axis of collimator plate.

Thus, the corresponding polar angle θ and azimuth angle ϕ of the observation direction are

$$\theta = \arccos\frac{z}{\sqrt{x^2+y^2+z^2}} = arccos\frac{\rho_2\cos\alpha_2 - \rho_1\cos\alpha_1}{\sqrt{t^2+\rho_1^2+\rho_2^2-2\rho_1\rho_2\cos(\alpha_2-\alpha_1)}}, \#(S5a)$$

and

$$\phi = \arctan\frac{y}{x} = \arctan\frac{\rho_2\sin\alpha_2 - \rho_1\sin\alpha_1}{t}. \#(S5b)$$

and the corresponding trigonometric functions that will be used in the following calculations include

$$\sin\theta = \frac{\sqrt{x^2+y^2}}{\sqrt{x^2+y^2+z^2}} = \frac{\sqrt{t^2+(\rho_2\sin\alpha_2 - \rho_1\sin\alpha_1)^2}}{\sqrt{t^2+\rho_1^2+\rho_2^2-2\rho_1\rho_2\cos(\alpha_2-\alpha_1)}}, \#(S6a)$$

$$\cos\phi = \frac{x}{\sqrt{x^2+y^2}} = \frac{t}{\sqrt{t^2+(\rho_2\sin\alpha_2 - \rho_1\sin\alpha_1)^2}}. \#(S6b)$$

The corresponding solid angle for collecting the scattering X-rays in this observation direction is

$$d\Omega = \sin\theta d\theta\, d\phi. \#(S7)$$

Therefore, the cross section of scattering X-rays that are emitted from dS_1 and detected by the entire S_2 is

$$\sigma_{coh,\ dS_1} = \iint_{S_2}\left(\frac{d\sigma}{d\Omega}\right)_{coh}(\theta,\phi)\cdot d\Omega(\theta,\phi) \#(S8a)$$

and

$$\sigma_{Comp,\ dS_1} = \iint_{S_2}\left(\frac{d\sigma}{d\Omega}\right)_{Comp}(\theta,\phi)\cdot d\Omega(\theta,\phi) \#(S8b)$$

As S_2 is more easily described by (ρ_2,α_2) rather than (θ,ϕ), it is necessary to find a *Jacobian* matrix to relate them. The

relation is given as

$$d\theta\, d\phi = \left\| \begin{matrix} \frac{\partial\theta}{\partial\alpha_2} & \frac{\partial\theta}{\partial\rho_2} \\ \frac{\partial\phi}{\partial\alpha_2} & \frac{\partial\phi}{\partial\rho_2} \end{matrix} \right\| d\alpha_2\, d\rho_2$$

$$= \frac{t\rho_2}{\left[t^2+\rho_1^2+\rho_2^2-2\rho_1\rho_2\cos\left(\alpha_2-\alpha_1\right)\right]\sqrt{t^2+\left(\rho_2\sin\alpha_2-\rho_1\sin\alpha_1\right)^2}} d\alpha_2\, d\rho_2 .\#(S9)$$

Then, the average cross section of the scattering from every point in the probing area S_1 on the sample is

$$\bar{\sigma}_{coh} = \frac{1}{S_1}\iint_{S_1} \sigma_{coh,\ dS_1} \cdot dS_1 ,\#(S10a)$$

$$\bar{\sigma}_{Comp} = \frac{1}{S_1}\iint_{S_1} \sigma_{Comp,\ dS_1} \cdot dS_1 .\#(S10b)$$

Consequently, for the parallel component in the primary X-ray beam, by combining the equations in (S1) and from (S3) to (S10), the final expression for the average cross section of coherent scattering is

$$\bar{\sigma}_{coh} = \frac{r_e^2}{\pi r^2}\int_0^r d\rho_1 \int_0^{2\pi} d\alpha_1 \int_0^r d\rho_2 \int_0^{2\pi} d\alpha_2 \frac{t\rho_1\rho_2\left[\rho_1^2+\rho_2^2-2\rho_1\rho_2\cos\left(\alpha_2-\alpha_1\right)\right]}{\left[t^2+\rho_1^2+\rho_2^2-2\rho_1\rho_2\cos\left(\alpha_2-\alpha_1\right)\right]^{\frac{5}{2}}} ,\#(S11a)$$

and the final expression for the average cross section of Compton scattering is

$$\bar{\sigma}_{Comp} = \frac{r_e^2}{\pi r^2}\int_0^r d\rho_1 \int_0^{2\pi} d\alpha_1 \int_0^r d\rho_2 \int_0^{2\pi} d\alpha_2 \cdot \left(\frac{k}{k_0}\right)^2 \left(\frac{k}{2k_0}+\frac{k_0}{2k}-\frac{t^2}{t^2+\rho_1^2+\rho_2^2-2\rho_1\rho_2\cos\left(\alpha_2-\alpha_1\right)}\right)$$
$$\times \frac{t\rho_1\rho_2}{\left[R^2+\rho_1^2+\rho_2^2-2\rho_1\rho_2\cos\left(\alpha_2-\alpha_1\right)\right]^{\frac{3}{2}}} .\#(S11b)$$

In a similar way, the average scattering cross sections for the perpendicular component in the primary X-ray beam are calculated. As shown in Fig. S4, the coordinates of the observation direction for the scattering X-rays from P_1 to P_2 are changed:

$$x' = \rho_2\sin\alpha_2 - \rho_1\sin\alpha_1 ,\#(S12a)$$
$$y' = t ,\#(S12b)$$
$$z' = \rho_2\cos\alpha_2 - \rho_1\cos\alpha_1 .\#(S12c)$$

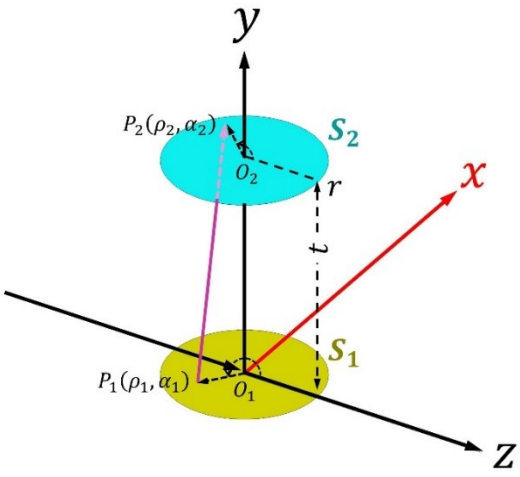

Figure S4. Calculation of perpendicular components in primary X-ray beam. Polarization is perpendicular to capillary axis of collimator plate.

By replacing the coordinates (x,y,z) in equations (S5) to (S10), the final expression for the average cross section of coherent scattering for the perpendicular component is

$$\bar{\sigma}'_{coh}=\frac{r_e^2}{\pi r^2}\int_0^r d\rho_1\int_0^{2\pi} d\alpha_1\int_0^r d\rho_2\int_0^{2\pi} d\alpha_2\frac{t\rho_1\rho_2\left[t^2+\left(\rho_2\cos\alpha_2-\rho_1\cos\alpha_1\right)^2\right]}{\left[t^2+\rho_1^2+\rho_2^2-2\rho_1\rho_2\cos\left(\alpha_2-\alpha_1\right)\right]^{\frac{5}{2}}},\#(S13a)$$

and the final expression for the average cross section of Compton scattering for the perpendicular component is

$$\bar{\sigma}'_{Comp}=\frac{r_e^2}{\pi r^2}\int_0^r d\rho_1\int_0^{2\pi} d\alpha_1\int_0^r d\rho_2\int_0^{2\pi} d\alpha_2\cdot\left(\frac{k}{k_0}\right)^2\left(\frac{k}{2k_0}+\frac{k_0}{2k}-\frac{\left(\rho_2\sin\alpha_2-\rho_1\sin\alpha_1\right)^2}{t^2+\rho_1^2+\rho_2^2-2\rho_1\rho_2\cos\left(\alpha_2-\alpha_1\right)}\right)$$
$$\times\frac{t\rho_1\rho_2}{\left[t^2+\rho_1^2+\rho_2^2-2\rho_1\rho_2\cos\left(\alpha_2-\alpha_1\right)\right]^{\frac{3}{2}}}.\#(S13b)$$

Finally, combining the coherent scattering cross section and the Compton scattering cross section for the parallel component and the perpendicular component, the final obtained average scattering cross section is

$$\bar{\sigma}=\frac{1+p}{2}\left(\bar{\sigma}_{coh}+\bar{\sigma}_{Comp}\right)+\frac{1-p}{2}\left(\bar{\sigma}'_{coh}+\bar{\sigma}'_{Comp}\right).\#(S14)$$

In the meantime, the effective solid angle Ω of the capillaries is given by

$$\Omega=\frac{1}{S_1}\iint_{S_2} d\Omega=\frac{1}{\pi r^2}\int_0^r d\rho_1\int_0^{2\pi} d\alpha_1\int_0^r d\rho_2\int_0^{2\pi} d\alpha_2\frac{t\rho_1\rho_2}{\left[t^2+\rho_1^2+\rho_2^2-2\rho_1\rho_2\cos\left(\alpha_2-\alpha_1\right)\right]^{\frac{3}{2}}}.\#(S15)$$

In this work, the integrations in (S11), (S12), and (S15) are numerically calculated by C#. The final obtained value of $\bar{\sigma}/\Omega$ is plotted with respect to the radius-to-length ratio of the capillaries and the DOP of the primary X-rays in Fig. 4 in

the article. In addition, it is noticed that $\bar{\sigma} \propto \Omega^2$ when r/t is small but still larger than the critical value in Fig. 4.

III. Simulation of X-ray fluorescence spectra

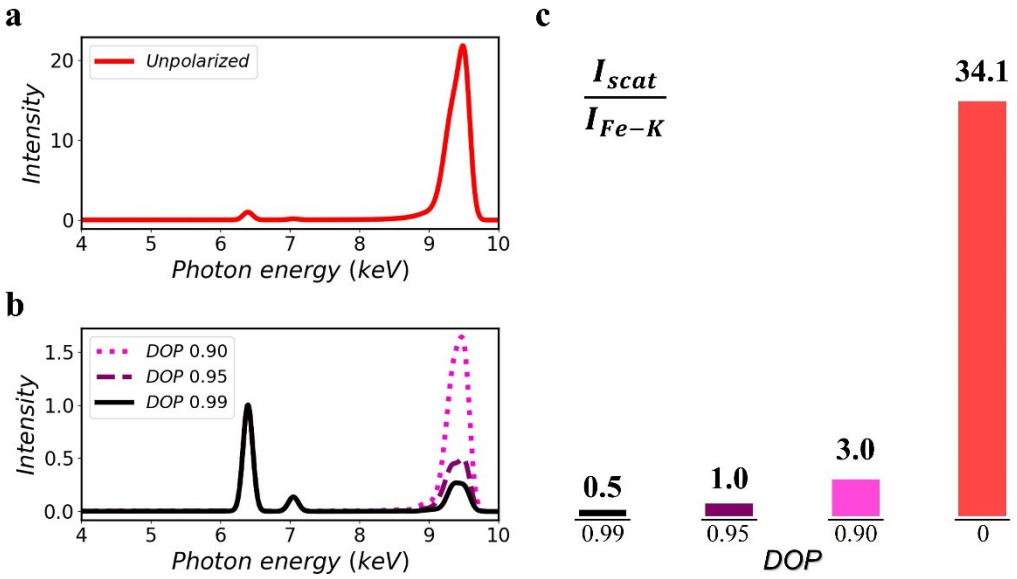

Figure S5. Simulated XRF spectra. Sample was cellulose pellet that included 100 ppm iron. Model for (a) resembles laboratory unpolarized experiment in this work, and model for (b) resembles synchrotron polarized experiment. For ease of comparison, primary X-ray energy in two models was set the same at 9.53 keV, and detector sensor thickness was set the same at 500 μm. (c) summarizes ratio of scattering intensity to iron K-line intensity in all spectra. Spectra in (a) are labeled as DOP = 0.

The simulated X-ray fluorescence spectra were generated by XMI-MSIM, which is an open-source tool developed by Tom Schoonjans, Laszlo Vincze and their co-workers. The software uses fundamental parameters in X-ray physics and Monto Carlo algorithms (further details are found in the documents on the Web page, https://github.com/tschoonj/xmimsim/wiki).

In the simulation, the sample was a cellulose pellet that included 100 ppm iron. The density of the cellulose matrix was 1.5 g/cm^3, and the thickness was 1 cm. There were two simulation models. In the model for Fig. S5(a), the geometry parameters were set the same as in the laboratory unpolarized experiment in this work. The primary X-rays were set as totally unpolarized for simplicity. In the model for Fig. S5(b), the geometry parameters were set the same as in the synchrotron polarized experiments. The radius-to-length ratio of collimation was 0.003. The DOP of the primary X-rays was set as 0.90, 0.95, and 0.99. For ease of comparison, in the two models, the primary X-ray energy was set at 9.53 keV to eliminate the influence of energy-dependent photon-matter interaction cross sections. The detector sensor thickness was set at 500 μm to eliminate the influence of the detection efficiency. In all spectra, the intensity on the *y*-axis was normalized by the peak height of iron Kα so that the huge difference of scattering intensity in the two models could be directly visualized. The ratio of the scattering intensity to the iron K-line intensity, which is inversely proportional to the signal-to-background ratio, is summarized and plotted in Fig. S5(c). Clearly, the collimator plate makes a great contribution to reducing the scattering background, especially when the DOP of the primary X-rays is high.